Three-dimensional pulsatile flow through a bifurcation

Chain-Nan Yung, Kenneth J. De Witt, Srikanth Subramanian, Abdollah A. Afjeh and Theo G. Keith

Departments of Chemical and Mechanical Engineering, The University of Toledo, Toledo, Ohio, USA

Received February 1996
Accepted April 1996

Introduction

The pattern of blood flow in arteries is complex near bifurcations, bends and stenoses. Study of such flow phenomena has drawn special attention of researchers because of the possible relation between the flow pattern and certain forms of arterial disease.

Clinical studies have shown that formation of atherosclerotic plaque and wall thickening in coronary arteries tends to localize in the vicinity of bifurcations and junctions (Asakura and Karino, 1990; Caro *et al.*, 1969). In this region, the sudden change of wall curvature can cause the forward-moving fluid to separate from the wall, resulting in a confined low velocity reversed flow region. Low fluid velocity was speculated to suppress mass transport between the mainstream and the wall and create a conducive environment for lipids to accumulate in the vessel walls. In addition, autoregulatory response to reversal of flow and wall shear stress could damage the mechanical properties of the endothelium. Laboratory tests have demonstrated the structural and functional changes in the endothelial cell exposed to fluid mechanical forces.

It is evident that hemodynamic factors play an important role in the development of atherosclerosis (Nerem, 1992; Nerem and Cornhill, 1980). Numerous studies have been carried out to investigate the fluid dynamic effects in bifurcations. Experimentally, Bharadvaj *et al.* (1982) and Ku and Giddens (1987) measured velocity and shear stress distributions in a model of the carotid bifurcation for steady and pulsatile flows. Walburn and Stein (1981) conducted a similar experiment in a symmetric bifurcation comparable to the human aorta. Most recently, Asakura and Karino (1990) examined flow patterns and distributions of fluid velocity and wall shear stress in an isolated human coronary arterial tree. They compared the results with the sites of

The authors express sincere appreciation to Dr Morton H. Friedman of the Biomedical Engineering Department at The Ohio State University for providing very helpful suggestions throughout the course of this work. We also thank the Ohio Supercomputer Center, Columbus, Ohio, for providing the computational time required for this study under project number PJS120.

International Journal of Numerical Methods for Heat & Fluid Flow
Vol. 7 No. 8, 1997, pp. 843–862.

atherosclerotic lesions and found that the lesions were exactly located in the low fluid velocity regions.

Compatible with the experimental studies, numerical simulation has provided detailed descriptions of flow in different bifurcation geometries. Early numerical analyses include Agonafer *et al.* (1985), Fernandez *et al.* (1976), Friedman and Ehrlich (1984) and Rindt *et al.* (1987) for flow in two-dimensional bifurcations. In recent years, the advance in computing technology has made numerical modelling of flow in three-dimensional bifurcations practical. Yung *et al.* (1990) studied the steady flow in a symmetric bifurcation for various upstream Reynolds numbers. They also traced the particle paths to examine if fluid particles would be entrapped in the recirculation zone. Rindt *et al.* (1990) analysed the steady flow in a carotid artery bifurcation. The flow patterns obtained were similar to those predicted by Perktold and Resch (1990), Perktold *et al.* (1991) and Yung *et al.* (1990), who simulated the pulsatile flow field in the same geometry used by Rindt *et al.* (1990). While Yung *et al.* (1990) used the finite difference technique for solving the governing equations, others used the finite element approach. The results from the three-dimensional simulations revealed the important effects of secondary flow, which cannot be predicted by a two-dimensional analysis.

The effect of unsteadiness on flow characteristics has been studied by Siouffi *et al.* (1984). The present study continues the work of Yung *et al.* (1990). In this study, the analysis is extended to model pulsatile flow in a full three-dimensional bifurcation using the finite difference technique. It is aimed to investigate the effects of inflow unsteadiness on flow characteristics such as recirculation, secondary motion, and wall shear stress distribution.

Mathematical model and numerical procedure

The problem considered here is the unsteady laminar flow of a homogeneous, incompressible, Newtonian fluid through a bifurcated channel with rigid walls. For constant density and viscosity, the dimensionless equations of continuity and momentum are:

$$\nabla . \underset{\sim}{u} = 0$$

$$\frac{\partial \underset{\sim}{u}}{\partial t} + \underset{\sim}{u} . \nabla \underset{\sim}{u} = -\nabla p + \frac{1}{Re} \nabla^2 \underset{\sim}{u}$$

where Re is the mean Reynolds number. The quantities are non-dimensionalized with respect to the inlet diameter of the channel and the mean inlet velocity. Non-slip boundary conditions are used at the walls by setting all the velocity components equal to zero. At the inlet, fully developed pulsatile laminar flow is applied. The axial velocity is varied with time according to the waveform of the pulsatile flow while the transverse velocities are set to zero. At the exit of the daughter tubes, a zero second derivative in the mean flow direction is imposed

on the velocities and pressure. The axial velocity obtained is adjusted to satisfy overall mass conservation.

The computational method follows that of Yung *et al.* (1990); therefore, only a brief discussion is given here. For the irregular bifurcation geometry, the body-fitted co-ordinate transformation is used to convert the curved flow domain into a rectangular computational domain. The governing equations of velocity and pressure in the transformed field are discretized by the control volume method and a hybrid difference scheme (Patankar, 1980) to form a set of algebraic equations. These equations express the relation between the variable at the centre of a control volume and its neighbouring points. The equations are solved using the pressure correction method (Patankar, 1980).

The geometry used is the same as in the previous analysis (Yung *et al.*, 1990). Figure 1 shows a perspective view of the bifurcation and Figure 2 illustrates the bifurcation geometry. The computation used $27 \times 17 \times 23$ nodal points in the x, y and z directions respectively. The grid nodes were generated for each z plane by solving a pair of Poisson equations subject to Dirichlet boundary conditions (Thomas and Middlecoff, 1980). The pulsatile flow waveform was taken from Bharadvaj *et al.* (1982) and assumed a mean Reynolds number of 400. Subdivision of the waveform into as many as 60 time steps produced the same calculated results as did 14 time steps. For computational efficiency, 14 time steps were therefore used, a selected four of which are designated as shown in Figure 3.

To start the calculation at each time step the inlet velocity is prescribed according to the position in the pulse cycle. The governing equations are solved iteratively until the maximum residue for all equations is below 10^{-3}. The residue is defined as the difference between the right and left hand sides of

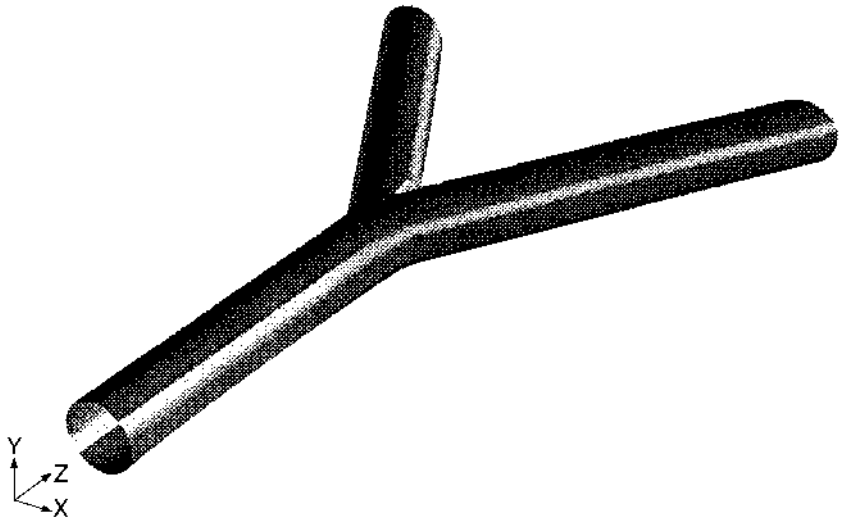

Figure 1.
Perspective view of the symmetric bifurcation model

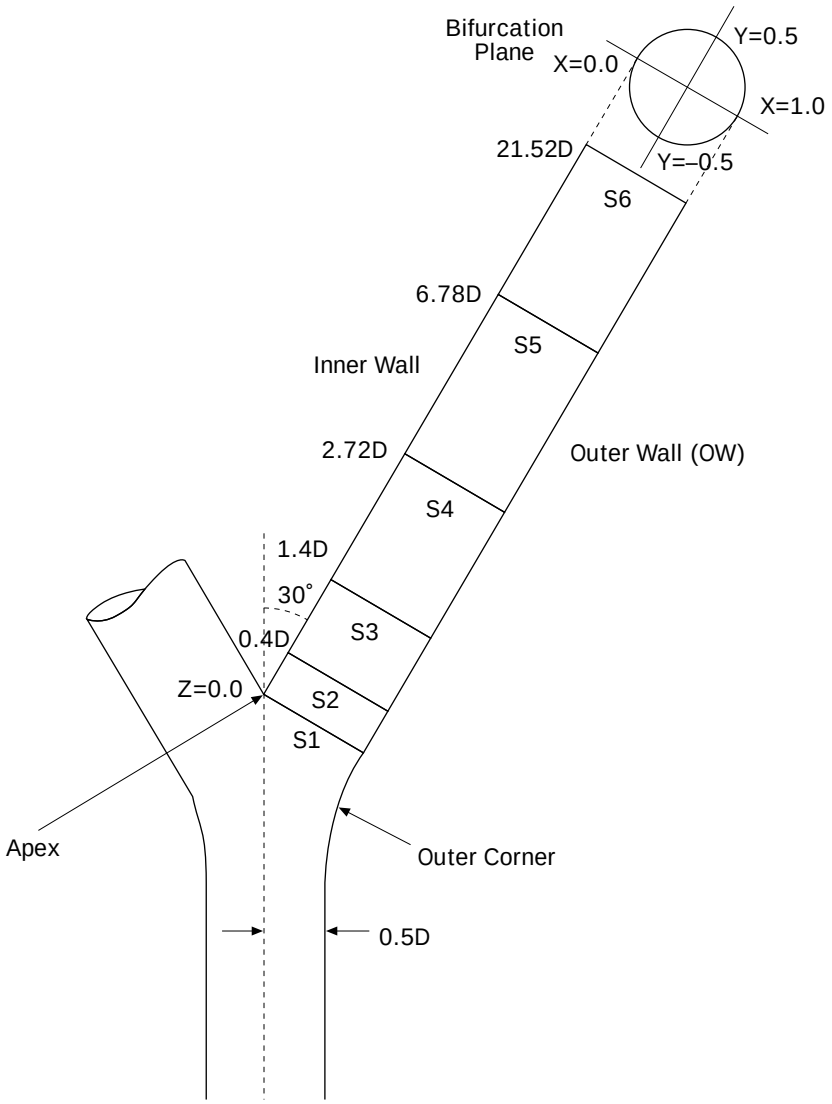

Figure 2.
Geometry of the bifurcation showing the six axial locations where the results are presented

the momentum equation divided by the inlet momentum. At the end of each time step, the mass flow rate through every z plane is checked. The maximum error as compared with the inflow is less than 0.1 per cent. Since the equations solved at the first time step would not have used the correct values for the variables at the previous time step, the computations have to be performed for more than one pulse cycle. For the current problem, the computations were performed for two complete cycles. At the end of the second cycle, the solutions were within 1 per cent of the previous cycle values. All computations were performed on the Ohio Supercomputer Center's Cray YMP8. The time

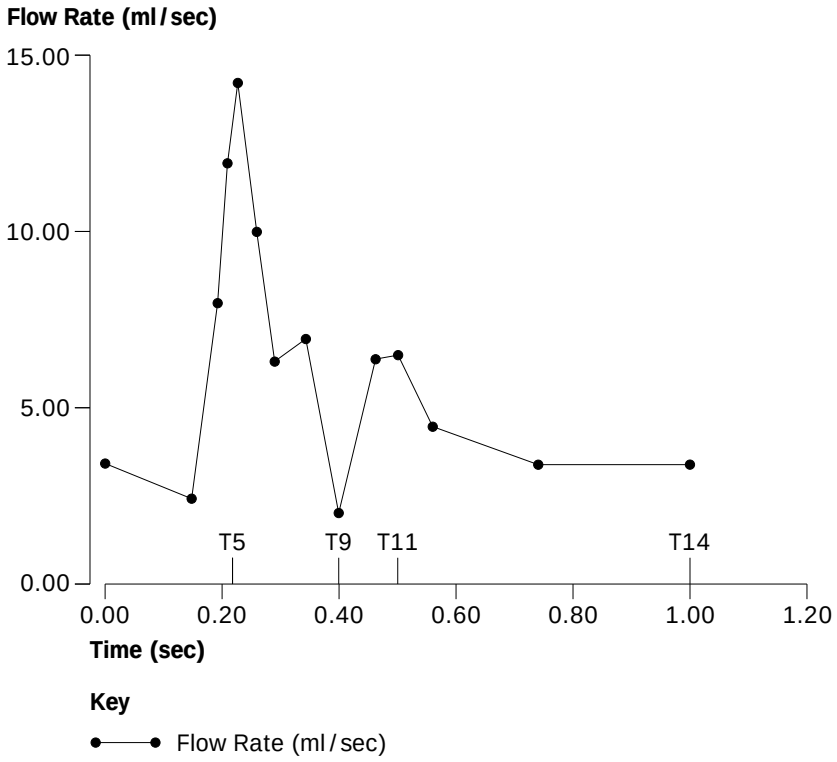

Figure 3. Pulsatile flow waveform in the common carotid artery as reported by Bharadvaj *et al.* (1982) with labels of the four time steps where the results are presented

required for one cycle of computations was approximately 12 CPU hours. This is comparable with 14 CPU hours on a CONVEX C1-XP machine reported by Perktold *et al.* (1991) for 98 time steps for a comparable mesh using the finite element method.

Results

The computed flow fields are presented for six downstream locations, labelled S1 to S6 in Figure 2, and for four different times, T5, 9, 11 and 14, as marked in Figure 3. These four time steps correspond to the maximum or peak systolic flow (Re = 1,250), the minimum flow (Re = 175), peak diastolic flow (Re = 580) and end (or start) of the pulse cycle (Re = 300) respectively.

Figures 4-7 are the three-dimensional axial velocity profiles at those time steps and positions. At the apex plane and immediately downstream of the bifurcation, stations S1 and S2, the velocity deflects towards the inner wall (flow-divider). The skewed velocity profile evens out downstream as seen in S5 and S6.

Figure 8 presents the velocity profiles in the bifurcation area for the four time steps. The profiles are plotted in the symmetric bifurcation plane ($y = 0$). When the flow enters the branches, the expansion of the flow area and the sharp wall curvature create an environment favouring an adverse pressure

gradient. During the acceleration phase of the pulse cycle, T1-T5, large flow rates supply enough energy to overcome the momentum deficit due to the change in the wall boundaries and no flow separation is found. This result agrees well with other numerical analyses (Nazemi *et al.*, 1990; Perktold and Hilbert, 1986). When the flow rate decreases during the deceleration phase of

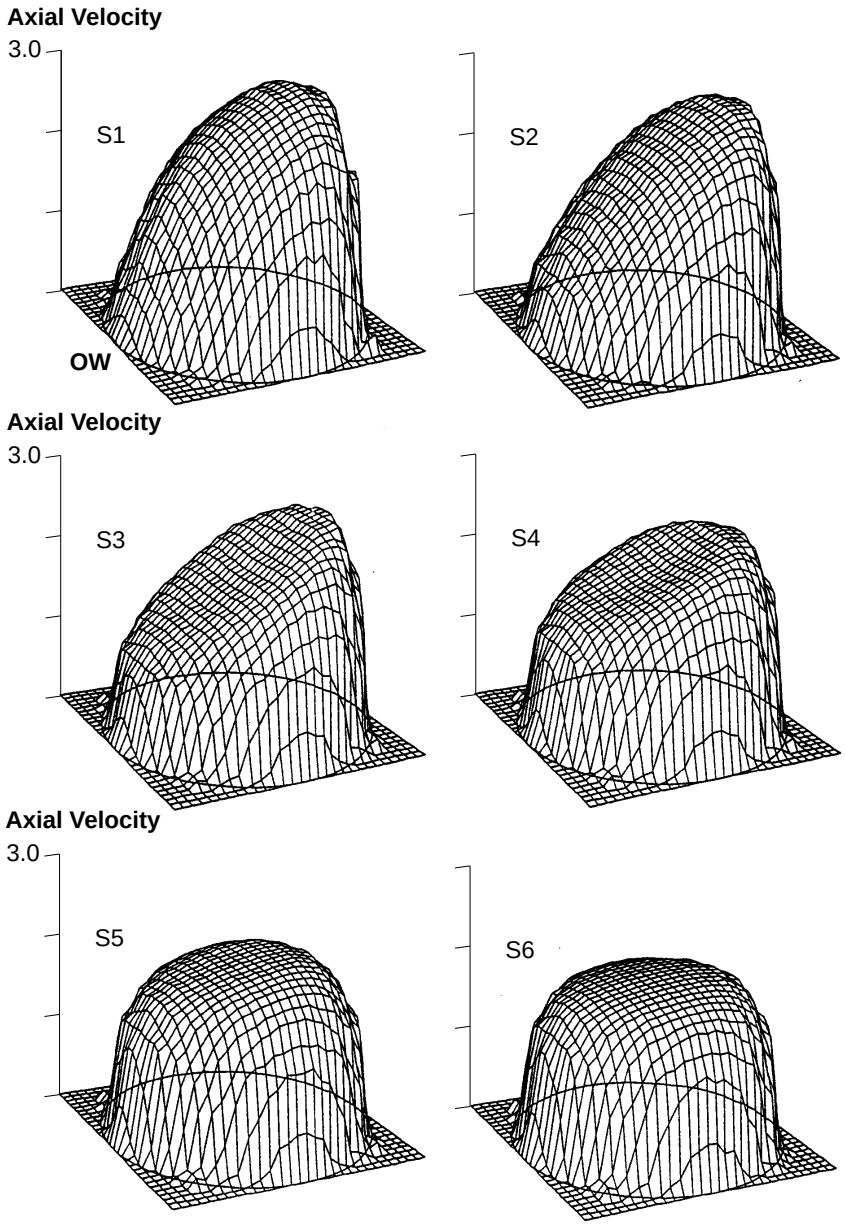

Figure 4.
Three-dimensional axial velocity profile at stations S1-S6 at time step T5 (peak systolic flow)

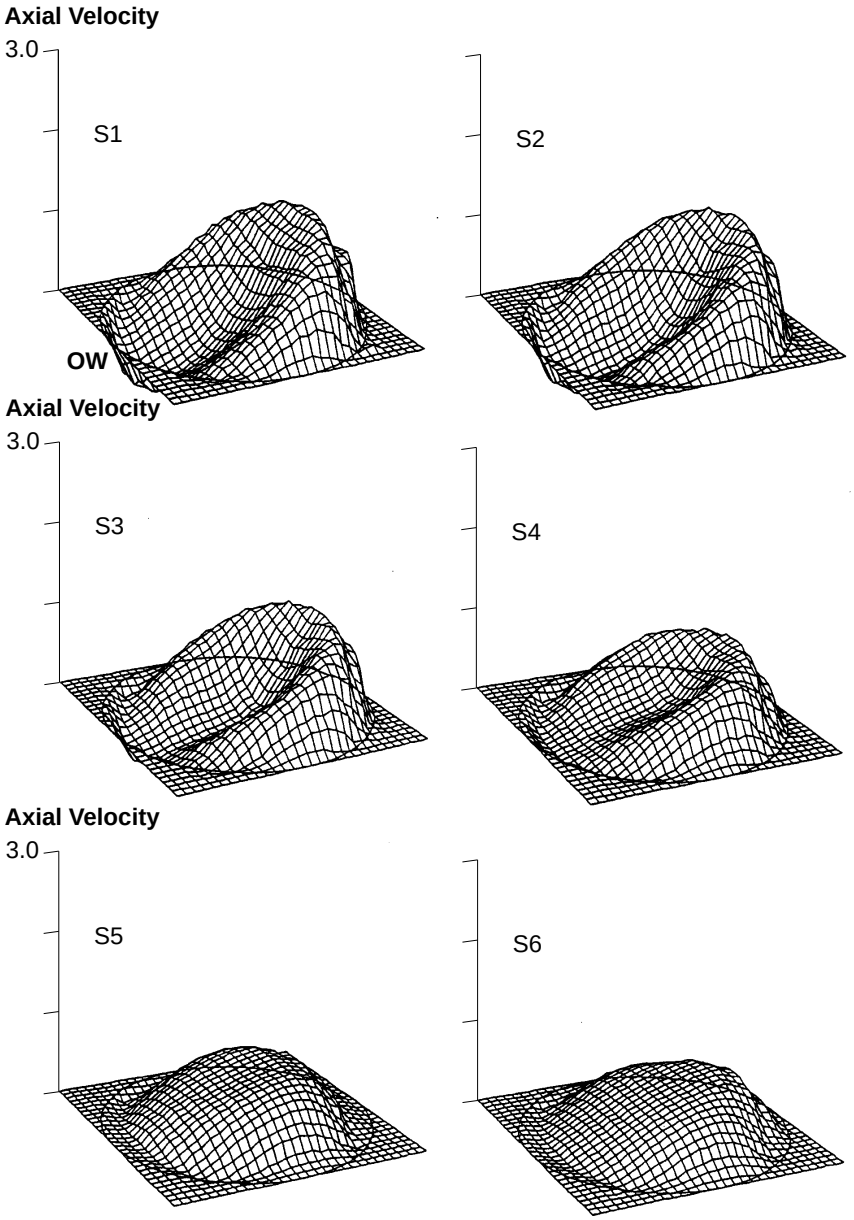

Figure 5.
Three-dimensional axial velocity profile at stations S1-S6 at time step T9 (minimum flow rate in pulse)

the pulse cycle, separation appears along the outer walls. The separation attains its maximum at the lowest flow rate at T9. As the flow reaches the diastole, T11, the increase of flow rate restores the axial flow momentum and flushes out most of the reversed flow region. In the rear half of the pulse, flow is decelerated, but a small recirculation zone remains. It vanishes in the middle of the next acceleration phase.

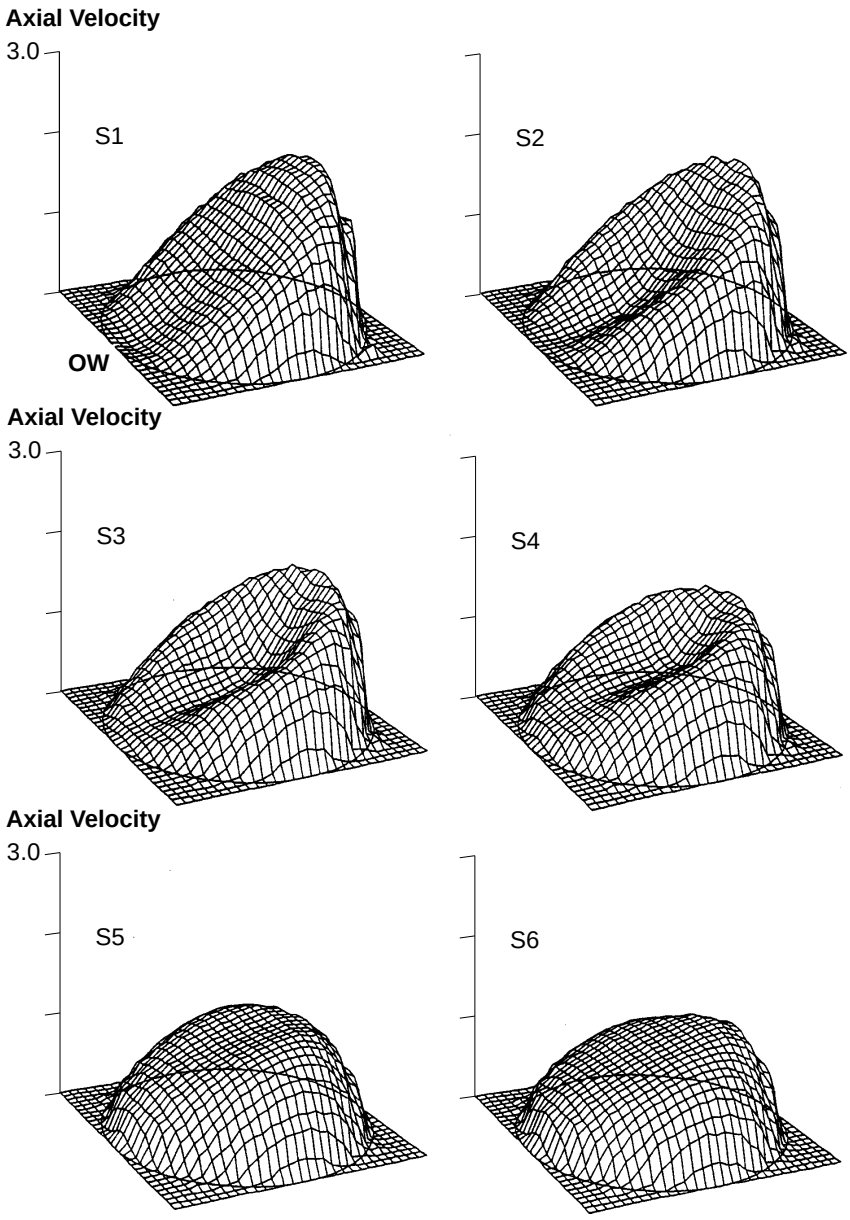

Figure 6.
Three-dimensional axial velocity profile at stations S1-S6 at time step T11 (peak diastolic flow)

The boundaries of the reverse flow region in the four vertical planes S1-S4 and in the bifurcation plane are depicted in Figures 9 and 10 respectively (note that no flow separation is observed at T5). The largest recirculation takes place at about a one diameter distance from the apex and is more than half a diameter in width. Table I lists the maximum forward and reversed dimensionless axial

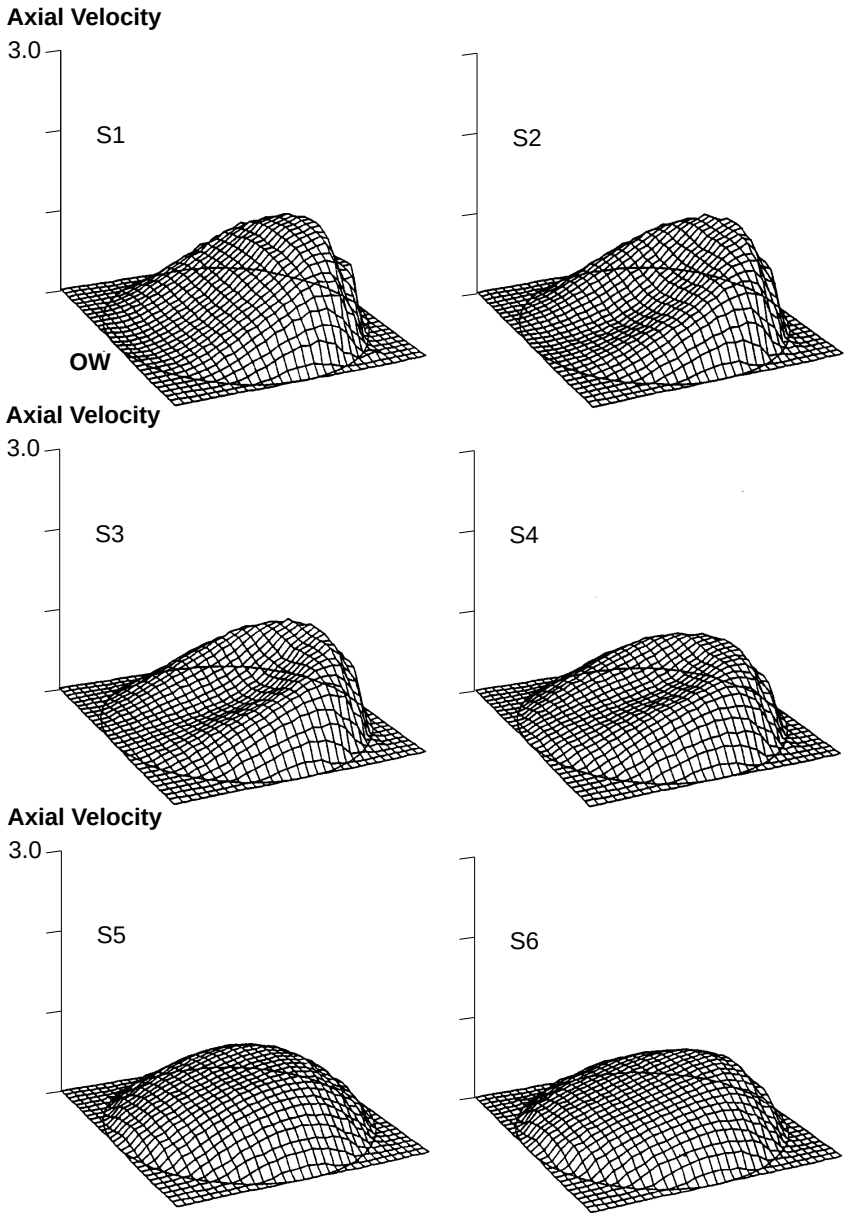

Figure 7.
Three-dimensional axial velocity profile at stations S1-S6 at time step T14 (start/end of cycle)

velocities at sections S1 and S2 for the four time steps. At T9, the magnitude of the reversed flow is nearly 50 per cent of the forward flow. However, at T11 and T14, it is drastically reduced to less than 3 per cent of the axial velocity.

It is noted that the recirculation zone formed at the lowest flow rate extends well upstream into the mother tube and downstream into the daughter tubes along the outer walls. The same phenomenon was also noticed in the work of

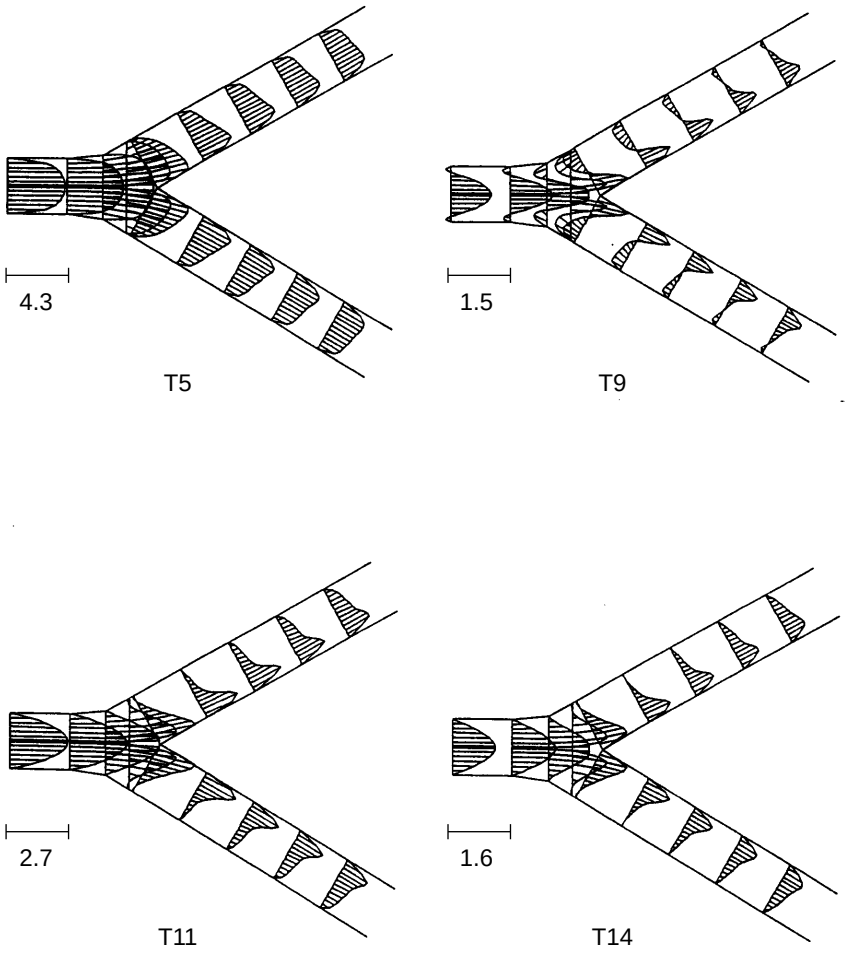

Figure 8.
Vector velocity plot in the bifurcation plane in the vicinity of the bifurcation for time steps T5, T9, T11 and T14

Nazemi *et al.* (1990) and Perktold and Resch (1990). In the experiment by Ku and Giddens (1987), the flow underwent a pulse cycle which did not have as large a drop in flow rate as in this analysis and the elongated separation was not observed. For the present pulse cycle, when the flow rate at time step T9 was raised to twice its original value, the extended flow separation disappeared. It is not known if this unusual flow separation will occur in physiological situations. In human arteries, it is more likely that the decrease in the flow rate will be accompanied by contraction of the vessel wall, thus preventing the large amount of reversed flow.

Secondary flow is brought about when the three-dimensional flow changes path or direction, such as in the bifurcation. The centrifugal force induced from this type of flow pushes the fluid towards the wall and causes a concavity in the velocity profiles as shown in Figures 4-7. The velocity vectors of the secondary flow at station S2 for various time steps are depicted in Figure 11.

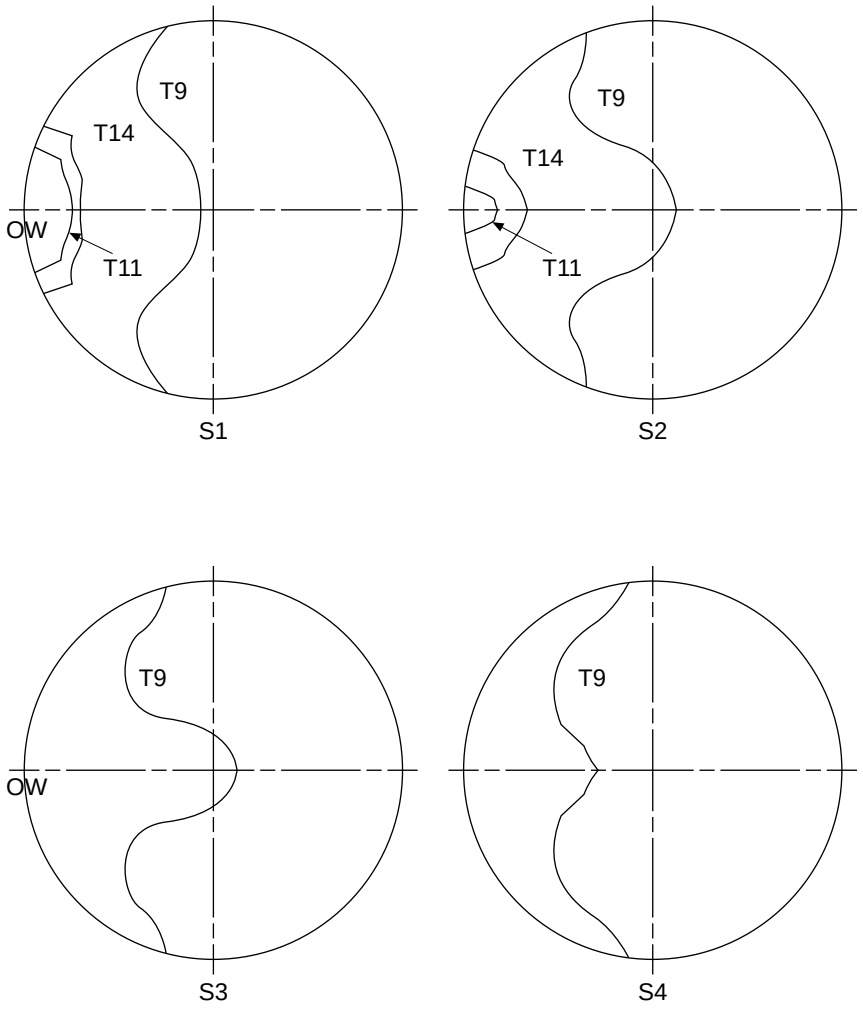

Figure 9.
Recirculation zones in the four vertical planes S1-S4 at the time steps T9, T11 and T14

The flow consists of two semi-circular streams which move in a spiral course from the apex to the outer edge along the upper and lower walls and return to the inner corner following a path parallel to the symmetric plane. The fluid particles are at a higher velocity when they approach the inner wall than when moving outward. Table II gives the maximum dimensionless transverse velocities at sections S1-S4 for various times. The ratio of the transverse velocity to the axial velocity is almost constant at each section, regardless of the flow rate. In this study, secondary flow was observed during the entire pulse cycle. Although similar results were reported in many experiments (Ku and Giddens, 1987), some did not observe the circumferential motion (Walburn and Stein, 1981) and some observed the circumferential motion only during the deceleration phase (Fukushima *et al.*, 1987). It may not be appropriate to make

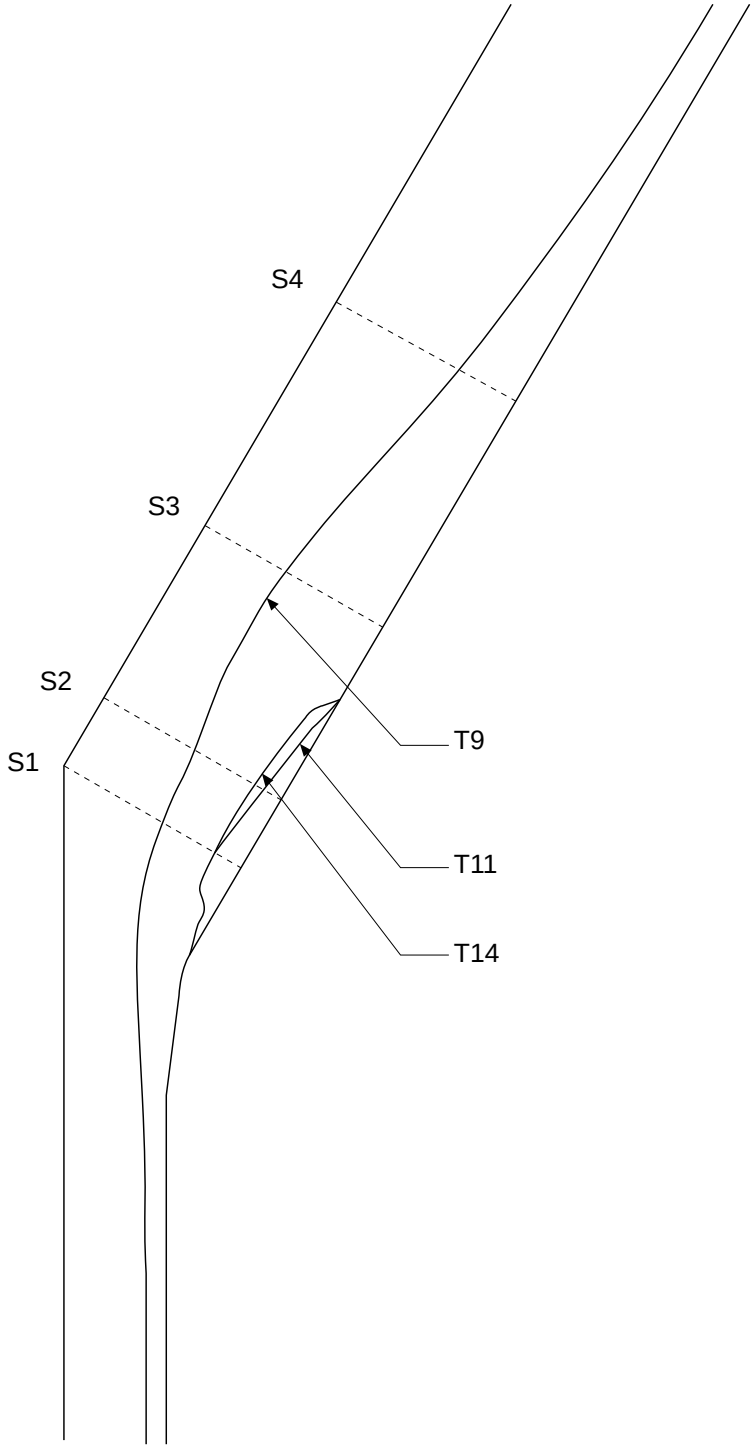

Figure 10.
Recirculation zones in the bifurcation plane at the time steps T9, T11 and T14

a direct comparison between these results because of the differences in geometries and conditions.

The shear stress along the outer and inner walls is presented in Figures 12 and 13 respectively. The magnitude of the shear stress is proportional to the

Time label	Maximum dimensionless velocity at S1		Maximum dimensionless velocity at S2	
	Axial	Reversed	Axial	Reversed
T5	2.807	–	2.656	–
T9	1.216	0.618	1.18	0.563
T11	1.885	0.058	1.82	0.007
T14	1.118	0.038	1.078	0.019

Table I.
Maximum forward and reversed dimensionless axial velocities

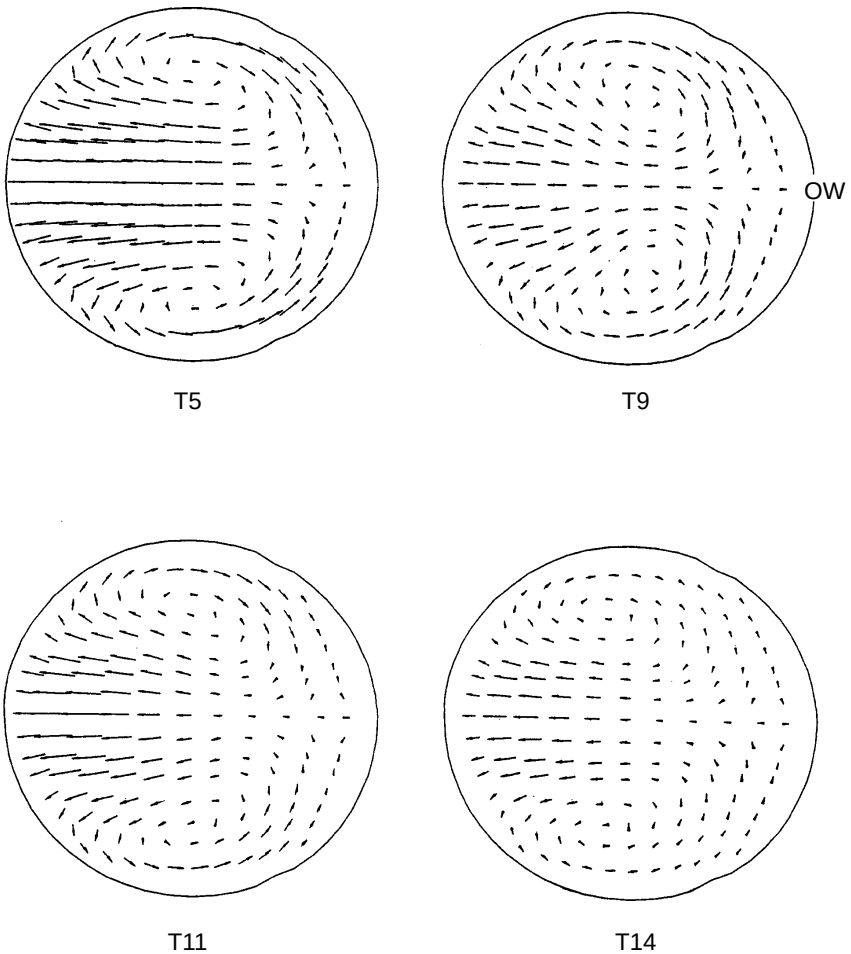

Figure 11.
Vector velocity plot of secondary flow at station S2 for time steps T5, T9, T11 and T14

instantaneous flow rate except at some locations where the flow is altered significantly. In the upstream region of the bifurcation, the constant shear stress indicates an undisturbed flow profile. Near the corner of the outer wall, the shear stress abruptly drops because of the sudden area increase. From the highest flow rate at T5 to the end of the diastole, T14, the wall shear stress in the outer corner region varies considerably. Along the flow divider or inner wall the shear stress has a similar pattern for all time steps. It reaches its maximum value at one diameter away from the apex and decreases to a minimum at ten diameters downstream followed by a small increase. The shear stress is calculated from the velocity gradient at the wall. Since a larger daughter-to-parent area ratio is used in this study, a lower averaged velocity and a smaller wall shear stress is predicted as compared to other analyses (Ku and Giddens, 1987; Perktold and Resch, 1990).

Table II.
Maximum dimensionless secondary velocities at stations

	Maximum dimensionless secondary velocity			
Time label	S1	S2	S3	S4
T5	0.763	0.454	0.212	0.102
T9	0.379	0.24	0.155	0.101
T11	0.558	0.347	0.156	0.094
T14	0.338	0.216	0.091	0.056

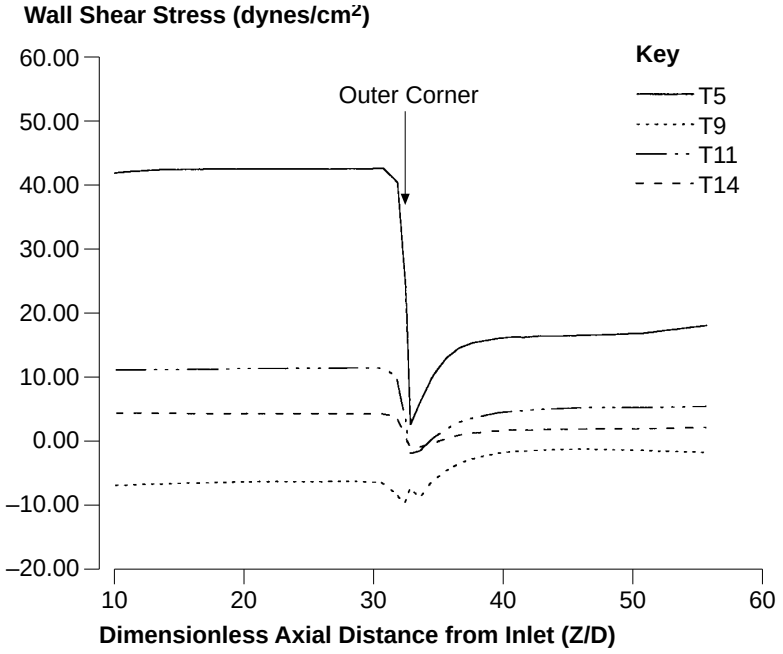

Figure 12.
Outer wall shear stress at time steps T5, T9, T11 and T14

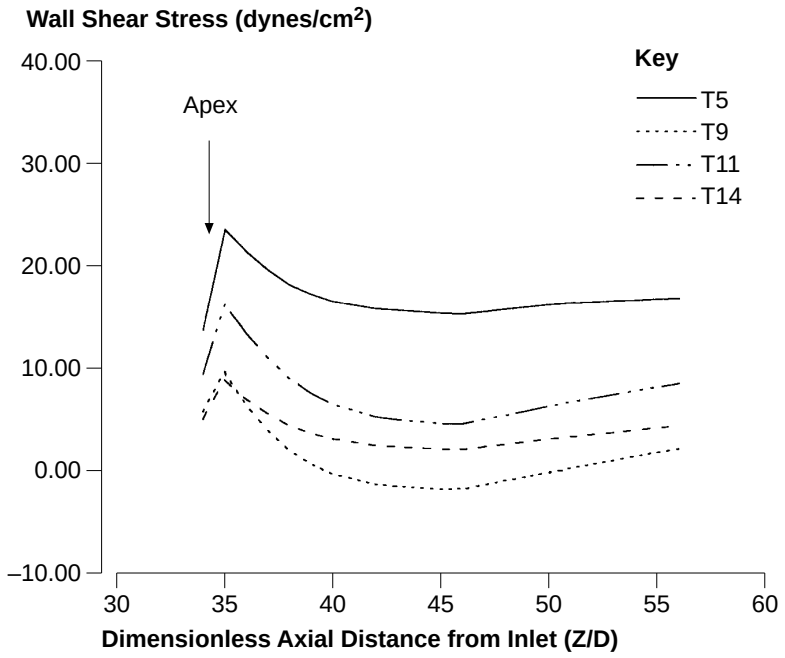

Figure 13. Inner wall shear stress at time steps T5, T9, T11 and T14

Discussion

Pulsatile flow through a bifurcation is characterized by unsteadiness, separation and secondary motion. The interaction of these mechanisms produces very complex flow phenomena. These complex flow patterns are believed to be directly related to the development of atherosclerosis. The present numerical study provides a quantitative picture of the pulsatile flow in a three-dimensional symmetric bifurcation. Although a quantitative comparison with experimental measurements in such a situation is not available, the flow pattern obtained is in qualitative agreement with experimental results (Ku and Giddens, 1987; Walburn and Stein, 1981).

The velocity profiles presented here show a marked change during the systolic phase. In the diastolic phase, the flow behaves steadily and the characteristics are more like steady flow. Flow separation and recirculation appear in distinct portions of the pulse cycle; they are located on the outer walls near the bifurcation entrance. Contrary to the steady state flow (Yung *et al.*, 1990), where the recirculation zone is augmented with increasing Reynolds number or flow rate, the pulsatile flow exhibits flow separation only under decelerating conditions. The size of the recirculation region varies with time and is enhanced by flow deceleration. At the lowest flow rate, the reversed flow region occupies half of the tube diameter. It is comparable in size to that obtained at steady state at the maximum flow rate of this waveform. Walburn and Stein (1981) postulated that the large flow reversal at the minimum flow rate was caused by the disappearance of the secondary

flow in the deceleration phase. Lack of secondary flow was also revealed in the experiments made by Brech and Bellhouse (1973) and Fukushima *et al.* (1987) during acceleration of the pulse cycle. These observations differ from the present analysis. The reason is mainly due to the different pulse waveforms and bifurcation geometries. The secondary flow exists at all times in this study. The strength of the transverse motion is proportional to the local axial flow velocity. The ratio varies from 0.3 at plane S1, to 0.1 at planes S3 and S4. These numbers are in line with those for steady flow at Reynolds numbers of 400 and 1,250, as presented in Table III. These results indicate that the formation of secondary flow depends on the bifurcation geometry and is not affected by the flow rate. The combination of the axial flow with the secondary flow forms a strong helical motion which pushes fluid from the mainstream to the recirculation area to ensure the exchange of materials between these two regions and remove the possibility of stagnated particles.

Wall shear stress is considered by many investigators to be the primary hemodynamic factor in the progress of atherosclerosis, e.g. Caro *et al.* (1969), Fry (1968), Sato *et al.* (1987) and Zarins *et al.* (1983). Fry (1968) reported that a shear stress of about 380dynes/cm^2 would damage the endothelium of the artery in a short period of time. Sato *et al.* (1987) also analysed the structural and mechanical properties of the bovine endothelium exposed to shear stresses from 10 to 85dynes/cm^2. They found a significant change in the structure of the cells in the monolayered endothelium. The endothelium cells were tightly packed when exposed to high shear and showed intercellular spaces under low shear stress. This might suggest that low shear regions may have a higher affinity for formation of lesions by allowing the influx of atherogenic molecules and may therefore be more conducive to the development of atherosclerosis. It has been shown that there is a positive correlation between the site of atherosclerotic lesions and low wall shear

Table III.
Maximum forward and reversed dimensionless axial velocities and maximum dimensionless secondary velocity at stations S1-S4 for steady flow at Re = 400 and 1,250

Location	Min. axial velocity	Max. axial velocity	Max. sec. velocity
Re = 400			
S1	–0.603	4.512	1.439
S2	–0.441	4.285	0.887
S3	0.000	3.709	0.444
S4	0.000	3.357	0.366
Re = 1,250			
S1	–0.055	1.412	0.426
S2	–0.023	1.364	0.272
S3	0.000	1.246	0.124
S4	0.000	1.058	0.079

stress (Asakura and Karino, 1990). For the geometry studied, the low shear region is identified in the vicinity of the bifurcation along the outer walls. In that region, the fluid moves very slowly and the flow changes direction regularly. The time averaged wall shear stress distributions on the outer and inner walls are shown in Figures 14 and 15 respectively. The steady state values at the mean Reynolds number, Re = 400, are also presented in the same figures for comparison. The difference in the outer wall shear stress in the upstream region between the time averaged and steady state values is due to the extended region of reverse flow in the unsteady problem at time step T9. At the inlet, the values are identical. The overall small difference in the shear stress and the transverse flow pattern between the steady and pulsatile flows suggests that these two types of flow are basically similar in nature.

In the lowest flow rate of the cycle, an extended reversed flow region was found. It is thought that the decrease of flow rate will be coupled with the movement of the vessel wall in a physiological situation to keep the flow from reversing. The effect of compliance of the arterial wall on the change of flow rate and the shear stress has been investigated (Deters *et al.*, 1986; Duncan *et al.*, 1990; Dutta *et al.*, 1992; Klanchar *et al.*, 1990; Liepsch and Moravec, 1984). Deters *et al.* (1986), measured the wall motion against the flow rate in a compliant arterial cast and found that the displacement of wall surface was in accordance with the flow rate. The surface moved outwards during the acceleration phase and moved inwards during deceleration. The

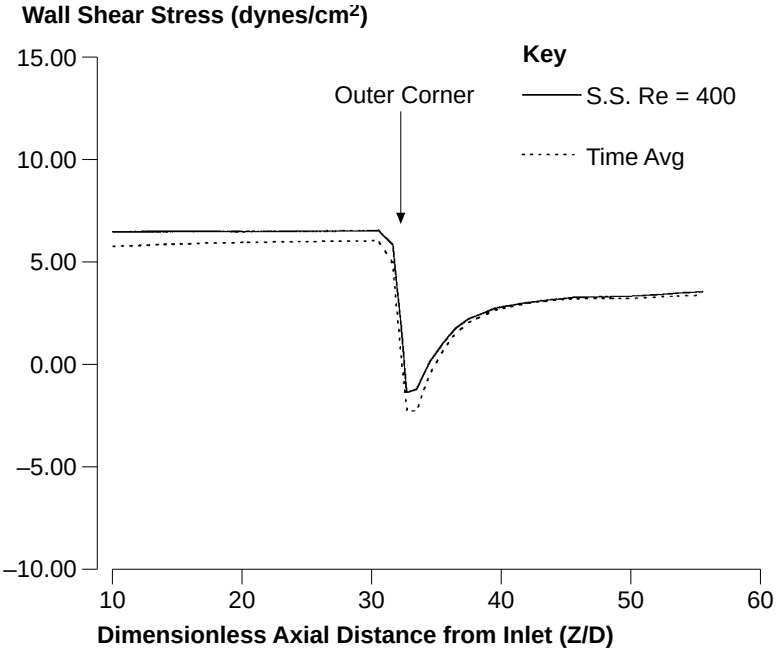

Figure 14. Comparison of time averaged and steady flow shear stress distributions along the outer wall

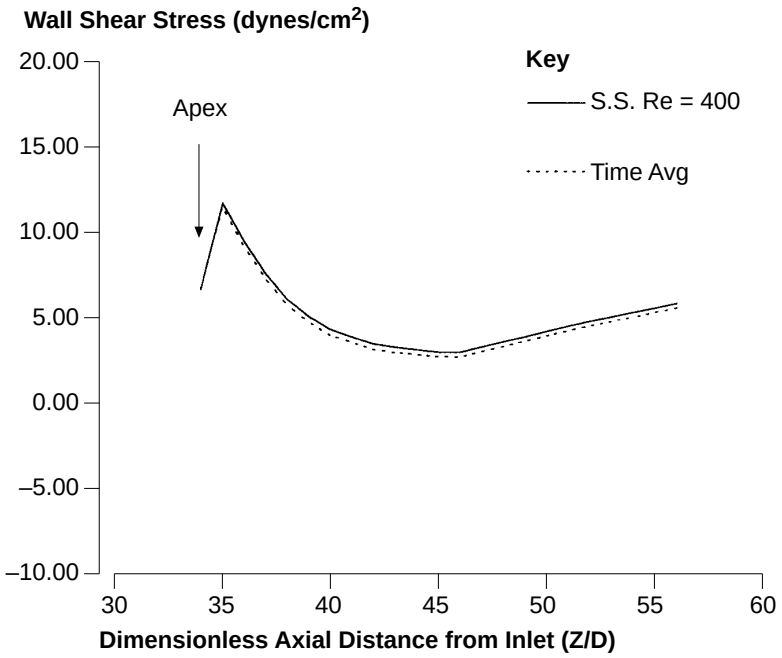

Figure 15.
Comparison of time averaged and steady flow shear stress distributions along the inner wall

effect of wall elasticity is recognized, but how that affects the wall shear stress has produced mixed results. Liepsch and Moravec (1984) reported a shear stress decrease of 25 per cent when the vessel wall was elastic. On the other hand, Mark *et al.* (1985) found 25 per cent elevation of the maximum shear stress in a compliant cast. More recently, Dutta *et al.* (1992) and Klanchar *et al.* (1990) observed that the wall shear stress was sensitive to the phase angle between the pressure and flow waves. They reported a fivefold increase in shear rate over a small phase angle range. The above studies underscore the importance of the wall movement. Nevertheless, the properties of vessel walls have not been considered in most of the numerical bifurcated flow simulation studies.

Summary

The three-dimensional pulsatile flow characteristics in a symmetrical bifurcation with a branch-to-trunk area ratio of 2.0 and a branching angle of 60° have been investigated numerically. The predicted flow profiles qualitatively resemble those obtained from experimental measurements. The flow recirculation appears only in the deceleration phase, and its size changes with time. The locations correspond well to the relation of low wall shear stress and the site of atherosclerosis. From a comparison of the pulsatile and steady flow results, the presence of the secondary flow is found to depend on the bifurcation geometry and not on the pulse wave or flow rate. It also shows that these two types of flow have similar flow characteristics, such as velocity

profile shape, size of recirculation, secondary flow and wall shear stress distribution.

References

Agonafer, D., Watkins, C.B. and Cannon, J.N. (1985), "Computation of steady flow in a two-dimensional arterial model", *Journal of Biomechanics,* Vol. 18, pp. 695-701.

Asakura, T. and Karino, T. (1990), "Flow patterns and spatial distribution of atherosclerotic lesions in human coronary arteries", *Circ. Res.*, Vol. 66, pp. 1,045-66.

Bharadvaj, B.K., Mabon, R.F. and Giddens, D.P. (1982), "Steady flow in a model of the human carotid bifurcation. Part I – flow visualization", *Journal of Biomechanics*, Vol. 15, pp. 349-62.

Brech, R. and Bellhouse, B.J. (1973), "Flow in branching vessels", *Cardiovasc. Res.,* Vol. 7, pp. 593-600.

Caro, C.G., Fitz-Gerald, J.M. and Schroter, R.C. (1969), "Arterial wall shear and distribution of early atheroma in man", *Nature,* Vol. 223, pp. 1,159-61.

Deters, O.J., Bargeron, C.B., Mark, F.F. and Friedman, M.H. (1986), "Measurement of wall motion and wall shear in a compliant arterial cast", *Journal of Biomechanical Engineering,* Vol. 108, pp. 355-8.

Duncan, D.D., Bargeron, C.B., Borchardt, S.E., Deters, O.J., Gearhart, S.A., Mark, F.F. and Friedman, M.H. (1990), "The effect of compliance on wall shear in casts of a human aortic bifurcation", *Journal of Biomechanical Engineering,* Vol. 112, pp. 183-8.

Dutta, A., Wang, D.M. and Tarbell, J.M. (1992), "Numerical analysis of flow in an elastic artery model", *Journal of Biomechanical Engineering,* Vol. 114, pp. 26-33.

Fernandez, R.C., De Witt, K.J. and Botwin, M.R. (1976), "Pulsatile flow through a bifurcation with applications to arterial disease", *Journal of Biomechanics,* Vol. 9, pp. 575-80.

Friedman, M.H. and Ehrlich, L.W. (1984), "Numerical simulation of aortic bifurcation flows: the effect of flow divider curvature", *Journal of Biomechanics,* Vol. 17, pp. 881-8.

Fry, D.L. (1968), "Acute vascular endothelial changes associated with increased blood velocity gradients", *Circ. Res.,* Vol. 22, pp. 165-97.

Fukushima, T., Homma, T., Azuma, T. and Harakawa, K. (1987), "Characteristics of secondary flow in steady and pulsatile flows through a symmetrical bifurcation", *Biorheology*, Vol. 24, pp. 3-12.

Klanchar, M., Tarbell, J.M. and Wang, D.M. (1990), "*In vitro* study of the influence of radial wall motion on wall shear stress in an elastic tube model of the aorta", *Circ. Res.,* Vol. 66, pp. 1624-35.

Ku, D.N. and Giddens, D.P. (1987), "Laser doppler anemometer measurements of pulsatile flow in a model carotid bifurcation", *Journal of Biomechanics,* Vol. 20, pp. 407-21.

Liepsch, D. and Moravec, St. (1984), "Pulsatile flow of non-Newtonian fluid in distensible models of human arteries", *Biorheology*, Vol. 21, pp. 571-86.

Mark, F.F., Deters, O.J., Bargeron, C.B. and Friedman, M.H. (1985), "Hermodynamic measurements of pulsatile flow through a compliant cast of a human aortic bifurcation",*Adv. Bioeng.*, pp. 59-60.

Nazemi, M., Kleinstreuer, C. and Archie, J.P. Jr, (1990), "Pulsatile two-dimensional flow and plaque formation in a carotid artery bifurcation", *Journal of Biomechanics,* Vol. 23, pp. 1,031-7.

Nerem, R.M. (1992), "Vascular fluid mechanics, the arterial wall and atherosclerosis", *Journal of Biomechanical Engineering,* Vol. 114, pp. 274-82.

Nerem, R.M. and Cornhill, J.F. (1980), "The role of fluid mechanics in atherogenesis", *Journal of Biomechanical Engineering,* Vol. 102, pp. 181-9.

Patankar, S.V. (1980), *Numerical Heat Transfer and Fluid Flow,* Hemisphere, Washington, DC.

Perktold, K. and Hilbert, D. (1986), "Numerical simulation of pulsatile flow in a carotid bifurcation model", *Journal of Biomedical Engineering*, Vol. 8, pp. 193-9.

Perktold, K. and Resch, M. (1990), "Numerical flow studies in human carotid artery bifurcations: basic discussion of the geometric factor in atherogenesis", *Journal of Biomedical Engineering,* Vol. 12, pp. 111-23.

Perktold, K., Resch, M. and Peter, R.O. (1991), "Three-dimensional numerical analysis of pulsatile flow and wall shear stress in the carotid artery bifurcation", *Journal of Biomechanics*, Vol. 24, pp. 409-20.

Rindt, C.C., van Steenhoven, A.A., Janssen, J.D., Reneman, R.S. and Segal, A. (1990), "A numerical analysis of steady flow in a three-dimensional model of the carotid artery bifurcation", *Journal of Biomechanics,* Vol. 23, pp. 461-73.

Rindt, C.C., van de Vosse, F.N., van Steenhoven, A.A., Janssen, J.D. and Reneman, R.S. (1987), "A numerical and experimental analysis of the flow field in a two-dimensional model of the human carotid artery bifurcation", *Journal of Biomechanics,* Vol. 20, pp. 499-509.

Sato, M., Levesque, M.J. and Nerem, R.M. (1987), "Micropipette aspiration of cultured bovine aortic endothelial cells exposed to shear stress", *Arteriosclerosis,* Vol. 7, pp. 276-86.

Siouffi, M., Pelissier, R., Farahifar, D. and Rieu, R. (1984), "The effect of unsteadiness on the flow through stenoses and bifurcations", *Journal of Biomechanics*, Vol. 17, pp. 299-315.

Thomas, D. and Middlecoff, J. (1980), "Direct control of grid point distribution in meshes generated by elliptic equations", *AIAA Journal,* Vol. 18, pp. 652-60.

Walburn, F.J. and Stein, P.D. (1981), "Velocity profiles in symmetrically branched tubes simulating the aortic bifurcation", *Journal of Biomechanics*, Vol. 14, pp. 601-11.

Yung, C.N., DeWitt, K.J. and Keith, T.G. Jr, (1990), "Three-dimensional steady flow through a bifurcation", *Journal of Biomechanical Engineering*, Vol. 112, pp. 189-97.

Zarins, C.K., Giddens, D.P., Bharadvaj, B.K., Sottiurai, V.S., Mabon, R.F. and Glagov, S. (1983), "Carotid bifurcation atherosclerosis: quantitative correlation of plaque localization with flow velocity profiles and wall shear stress", *Circ. Res.,* Vol. 53, pp. 502-14.